

Current Generation by Unidirectional Lower Hybrid Waves in the ACT-1 Toroidal Device

King-Lap Wong, Robert Horton, and Masayuki Ono

Plasma Physics Laboratory, Princeton University, Princeton, New Jersey 08544

(Received 28 April 1980)

An unambiguous experimental observation of current generation by unidirectional lower hybrid waves in a toroidal plasma is reported. Up to 10 A of current was driven by 500 W of rf power at 160 MHz.

PACS numbers: 52.55.Gb, 52.35.Hr

All existing tokamaks are capable only of pulsed operation, since the toroidal plasma current is driven by an inductive method. Obvious advantages of a steady-state tokamak reactor include a longer first-wall life in the absence of cyclic thermal and mechanical excursions; elimination of a thermal storage system for continuous power production; and removal of the Ohmic heating coils. A steady-state current can be driven by radio-frequency waves,¹⁻⁹ but if the current is carried by the main-body electrons, the rf power required is too large to be practical.⁴ Far less rf power is required if the current is carried by the electrons in the tail of the distribution function. This can be accomplished via Landau damping of the lower hybrid wave.^{8,9} In this paper, we report the first unambiguous experimental observation of current generation by unidirectional lower hybrid waves in a toroidal plasma.

Consider a lower hybrid wave propagating in a magnetized plasma ($\vec{B}_0 = B_0 \hat{z}$) with parallel phase velocity ω/k_z . The wave obeys the electrostatic dispersion relation:

$$\epsilon(\vec{k}, \omega) = 1 - \frac{\omega_{pe}^2}{\omega^2} - \frac{\omega_{pe}^2 k_z^2}{\omega^2 k^2} + \frac{\omega_{pe}^2 k_{\perp}^2}{\omega_{ce}^2 k^2} = 0. \quad (1)$$

To calculate the current generated by the wave, one can study the evolution of the space-averaged electron distribution function $f(v_z, t)$ in the presence of rf waves by the one-dimensional Fokker-Planck equation^{9,10}:

$$\frac{\partial f}{\partial t} = \frac{\partial}{\partial v_z} D_{\text{rf}} \frac{\partial}{\partial v_z} f + \left(\frac{\partial f}{\partial t} \right)_c, \quad (2)$$

where D_{rf} is the quasilinear diffusion coefficient, and $(\partial f / \partial t)_c$ is the collision term. The rf-generated current can be calculated from the steady-state solution of Eq. (2). Let us assume that $D_{\text{rf}}(v_z) = \infty$ for $v_1 < v_z < v_2$ and zero elsewhere; then $f(v_z)$ plateaus for $v_1 < v_z < v_2$ and this gives rise to a current in the plasma. Let E_0 denote the amplitude of the wave electric field; then,

the total plasma current density is

$$J = \frac{ne}{(2\pi kT/m)^{1/2}} \frac{v_z^2 - v_1^2}{2} \exp\left(-\frac{mv_z^2}{2kT}\right) + \frac{n_z^2 - 1}{n_z^2} \frac{e E_0^2 k_z}{m 8\pi \omega} \left(1 + \frac{\omega_{pe}^2}{\omega_{ce}^2}\right), \quad (3)$$

where n , T , and n_z denote the electron density, the electron temperature, and the wave parallel index of refraction. The first term in Eq. (3) is due to the resonant electrons in the plateau of $f(v_z)$ and the second term (usually small compared with the first term) is due to the nonresonant electrons which support the wave. It is apparent that after $f(v_z)$ plateaus, additional rf power can only raise the current density via the second term in Eq. (3).

In order to optimize the current generation efficiency, one has to confine the current-carrying electrons inside the torus. Because of the magnetic field-line curvature and the field gradient, electrons can leave the torus by drifting across the magnetic field (vertically downward in ACT-1) with the drift velocity

$$\vec{V}_d = \frac{v_z^2}{\omega_{ce}} \frac{\vec{R} \times \vec{B}_0}{R^2 B_0} + \frac{v_{\perp}^2}{2\omega_{ce}} \frac{\vec{B}_0 \times \nabla B_0}{B_0^2}. \quad (4)$$

These electrons can be confined in the torus by adding a small vertical magnetic field

$$\vec{B}_v = (V_d / v_z) B_0 \vec{R} \times \vec{v}_z / |\vec{R} \times \vec{v}_z|, \quad (5)$$

so that the vertical component of \vec{v}_z cancels the drift velocity \vec{V}_d . Here \vec{R} denotes the radius of curvature of the field line and ω_{ce} is the electron cyclotron frequency. Note that the direction of \vec{B}_v changes with the direction of \vec{v}_z .

The idea of lower-hybrid-wave current drive relies upon momentum transfer from the waves to the resonant electrons and therefore requires unidirectional waves which can be generated by 90° phased metal plates or waveguide arrays. Excitation of unidirectional waves and momentum transfer from waves to tail electrons have been experimentally demonstrated¹¹ in the Princeton

L-3 linear device. In a toroidal device, the current-carrying electrons are confined and therefore the current generation efficiency (amperes/watt) should be much better. The experimental data reported in this paper demonstrate an order-of-magnitude increase in current-drive efficiency compared with previous linear machine results.^{6, 11}

The experiment was performed in the Princeton ACT-1 device¹² (Advanced Concepts Torus I), a new toroidal machine designed primarily for rf heating and rf current generation research. It has a pure toroidal magnetic field without rotational transform. The plasma equilibrium is maintained by a small vertical current which flows to the limiter and completes the electrical circuit. Figure 1 shows the schematic of the device. The experiment was performed with the following plasma parameters: plasma density $n \sim 2 \times 10^{10} \text{ cm}^{-3}$, electron temperature $T_e \sim 5 - 10 \text{ eV}$, ion temperature $T_i \sim 0.5 \text{ eV}$, toroidal magnetic field $B_0 \approx 3 \text{ kG}$ on the minor axis, neutral pressure $p_0 \sim 8 \times 10^{-5} \text{ Torr}$, plasma radius $\sim 9 \text{ cm}$. The helium plasma was produced by 200 W of rf heating near the electron cyclotron frequency (9 GHz), and also by a hot tungsten filament inserted into the torus. Lower hybrid waves at 160 MHz were launched by two sets of antennas of parallel wavelengths 5.1 and 7.6 cm. Each set of antennas consists of four electrostatic rings with a 90° phase difference between the rf voltage applied on adjacent rings. Figure 2(a) shows the schematic of the rf network. In order to verify the directionality of the antenna, the radial profile of the

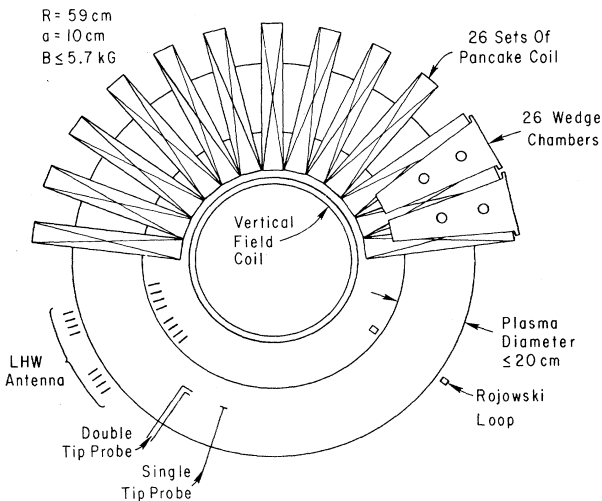


FIG. 1. Schematic of the ACT-1 device.

wave amplitude was measured with a double-tip probe one port away from the antenna and the result is shown in Fig. 2(b). When the antenna phasing is chosen to launch a wave propagating towards the probe, the wave amplitude detected by the probe is much larger than when the wave is launched away from the probe. The two peaks in the amplitude profile correspond to the resonance cones emanating from the two sets of antennas. Interferometry measurements of the wavelength show that the wave satisfies the dispersion relation [Eq. (1)]. The current generated by the wave was measured by a 1000-turn Rogowski loop as shown in Fig. 3(a). The Rogowski loop sensitivity (1.3 mV/A) and the response time ($\sim 0.3 \mu\text{s}$) was experimentally determined by sending a known pulsed current through the loop. Fig-

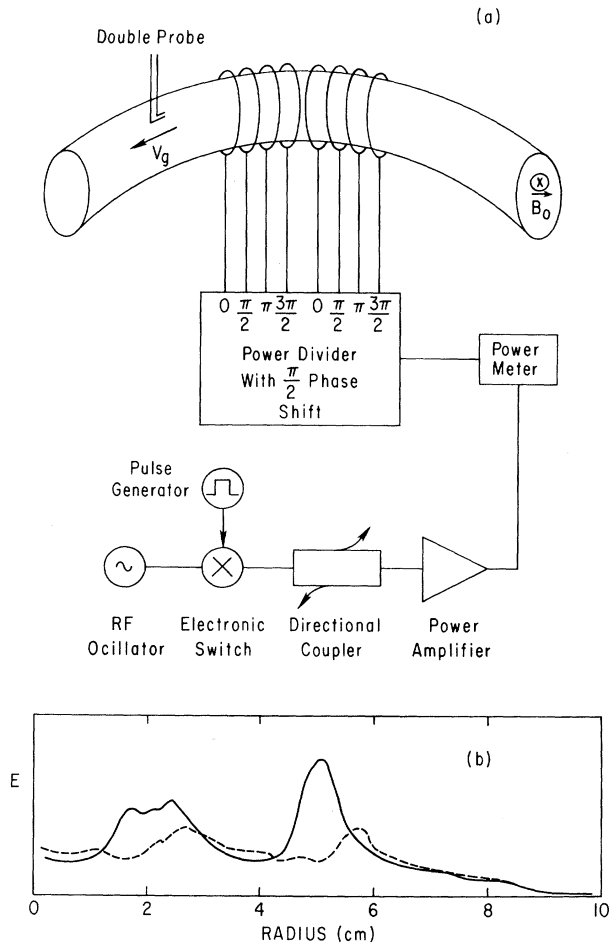
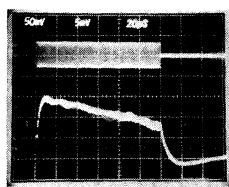
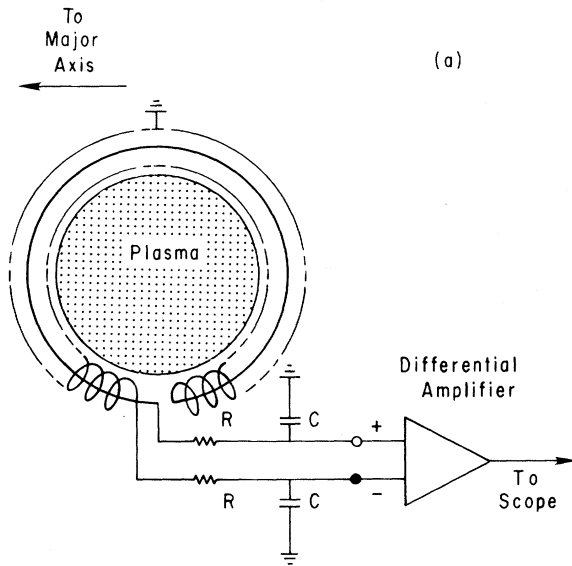
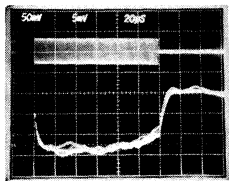


FIG. 2. (a) Schematic of the rf network for wave excitation. (b) Radial profiles of the wave amplitude when the wave is launched towards the probe (solid line) and away from the probe (dotted line).



(b) $\vec{V}_g \cdot \vec{B}_0 > 0$



(c) $\vec{V}_g \cdot \vec{B}_0 < 0$

FIG. 3. (a) Integrated Rogowski loop for current measurements. (b) Current generated by a 200-W, 120- μ s rf pulse with $\vec{V}_g \cdot \vec{B}_0 > 0$. (\vec{V}_g denotes the group velocity of the wave.) Top trace shows the rf pulse and bottom trace shows the Rogowski-loop signal. (c) Same, but with $\vec{V}_g \cdot \vec{B}_0 < 0$.

ures 3(b) and 3(c) show that, as expected, the rf-generated current changes direction when the wave propagation is reversed. One should note that the RC time constant of the Rogowski loop signal is 100 μ s and the slowly varying current signal in Fig. 3(b) and 3(c) is due to the droop of the RC integrator. The oscillograms show overlay of four consecutive pulses which demonstrate the reproducibility of the experiment. The outer half of the Rogowski loop picks up a signal larger than the inner half, indicating that the current profile

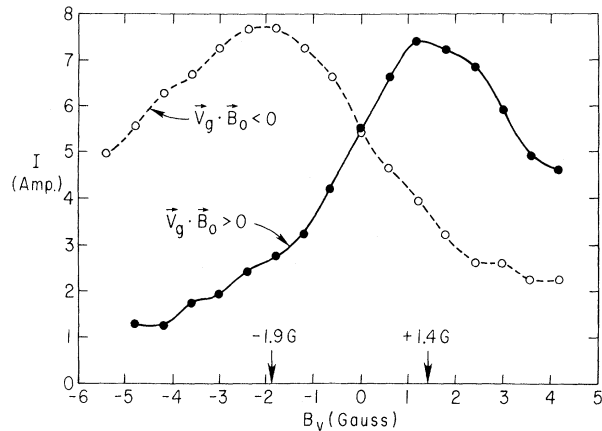


FIG. 4. Variation of rf-generated current I with vertical magnetic field \vec{B}_v . The currents flow in opposite directions for the two cases ($\vec{V}_g \cdot \vec{B}_0 > 0$ and $\vec{V}_g \cdot \vec{B}_0 < 0$). Only the magnitudes of the currents are plotted here for easy comparison.

peaks outside the minor axis. Up to 10 A of current has been driven by 500 W of rf power. Calculation of the rf-generated current requires an accurate value of $f(v_1)$. Put $T = 8$ eV, $f_0 = 160$ MHz, $\lambda_1 = 5.1$ cm, $\lambda_2 = 7.6$ cm, $v_1 = \frac{1}{2}f_0\lambda_1$, $v_2 = \frac{3}{2}f_0\lambda_2$, $n = 2 \times 10^{10}$ cm $^{-3}$; then Eq. (3) predicts $I \sim 10$ A which is in rough agreement with experiment. It should be noted that Eq. (3) can only give an order-of-magnitude estimate because of the uncertainties in $f(v_1)$, v_1 , v_2 , and the profile effects.

A small vertical magnetic field \vec{B}_v (up to 10 G on the minor axis) can be applied by two 80-turn coils situated inside the bore of the torus. The spiraling magnetic field line was traced out by a tenuous 100-eV electron beam emitted from a small electron gun. The value of \vec{B}_v determined from the pitch of the helical field line and the toroidal field \vec{B}_0 is in excellent agreement with the measurements by a Hall-probe gaussmeter. Figure 4 shows the variation of the rf-generated current with the vertical field \vec{B}_v (values taken on the minor axis). As expected from Eq. (5), the optimum value of \vec{B}_v changes direction when the wave propagation direction is reversed. If we put $v_g = 10^9$ cm/sec which is the average parallel phase velocity of the waves and assume $v_{\perp}^2 \ll v_g^2$, Eqs. (4) and (5) predict an optimum $B_v \approx 1$ G which is in reasonable agreement with the experimental results presented in Fig. 4. The discrepancy can be qualitatively explained by the fact that the current peaks outside the minor axis of the torus. If v_{\perp} is substantial fraction of v_g because of collisions, then Eq. (6) will predict a

B_v larger than 1 G also.

The authors would like to thank Dr. T. Stix, Dr. N. Fisch, Dr. H. Furth, Dr. W. Hooke, Dr. C. Karney, and Dr. R. Motley for helpful discussions and their continuous interest in this experiment. Technical assistance by Mr. W. Kineyko, J. Taylor, and J. R. Wilson is gratefully appreciated.

This work was supported by the U. S. Department of Energy under Contract No. DE-AC02-76-CH03073.

¹D. J. H. Wort, *Plasma Phys.* **13**, 258 (1971).

²M. Fukuda, K. Matsuura, K. Hirano, A. Mohri, and M. Fukao, *J. Phys. Soc. Jpn.* **41**, 1376 (1976).

³S. Yoshikawa and H. Yamato, *Phys. Fluids* **9**, 814 (1966).

⁴T. Ohkawa, *Nucl. Fusion* **10**, 185 (1970).

⁵R. Klima, *Plasma Phys.* **15**, 1031 (1973).

⁶R. McWilliams, E. J. Valeo, R. W. Motley, W. M. Hooke, and L. Olsen, *Phys. Rev. Lett.* **44**, 245 (1980).

⁷R. J. LaHaye, C. J. Armentroat, R. W. Harvey, C. P. Moeller, and R. D. Stambaugh, *Nucl. Fusion* **20**, 218 (1980).

⁸A. Bers and N. Fisch, in *Proceedings of the Third Topical Conference on Radio Frequency Plasma Heating*, Pasadena, California, 1978 (unpublished), papers E-5 and E-6.

⁹N. J. Fisch, *Phys. Rev. Lett.* **41**, 873 (1978).

¹⁰Charles F. F. Karney and Nathaniel J. Fisch, *Phys. Fluids* **22**, 1817 (1979). This paper shows that two-dimensional velocity space effects only give a minor quantitative difference from one-dimensional analytic results.

¹¹K. L. Wong, *Phys. Rev. Lett.* **43**, 438 (1979).

¹²K. L. Wong and M. Ono, *Bull. Am. Phys. Soc.* **24**, 957 (1979).

Ni on Si(111): Reactivity and Interface Structure

N. W. Cheung

California Institute of Technology, Pasadena, California 91109, and Bell Laboratories, Murray Hill, New Jersey 07974

and

R. J. Culbertson, L. C. Feldman, P. J. Silverman, and K. W. West

Bell Laboratories, Murray Hill, New Jersey 07974

and

J. W. Mayer

California Institute of Technology, Pasadena, California 91109

(Received 7 March 1980)

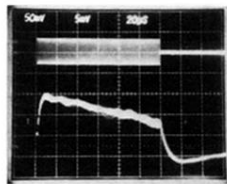
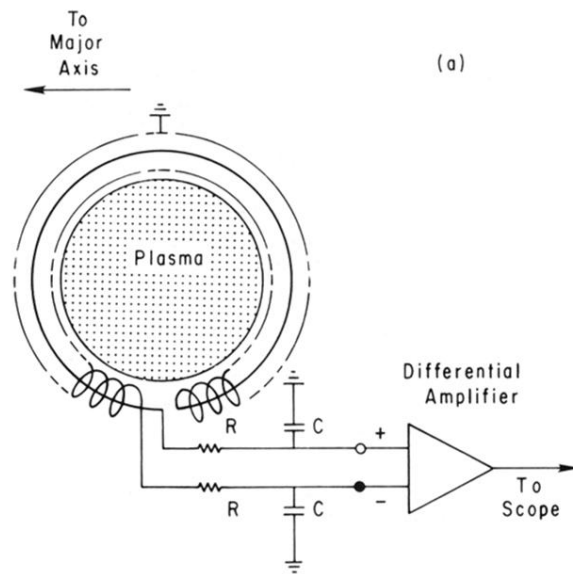
The megaelectronvolt ion-channeling technique has been applied to the study of the Ni-Si interface. The Ni-Si interface, prepared under UHV conditions at ambient temperature, shows an interfacial region containing $\sim 1 \times 10^{16}$ atoms/cm² of nonregistered Si. A measurement of the temperature dependence of the interfacial reactivity emphasizes the kinetic nature of the Ni-Si interface and the importance of Schottky-barrier height measurements at low temperatures for meaningful comparison with abrupt metal-semiconductor interface models.

PACS numbers: 68.48.+f, 61.80.Mk, 73.40.Ns

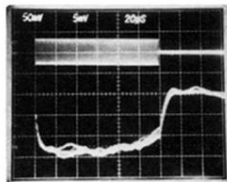
The understanding of the structure and bonding at the metal-semiconductor interface is essential for a theoretical description of Schottky barrier heights.¹⁻⁴ In the simplest approximation this system has been modeled as an abrupt interface. Recently, however, it has been observed that changes in the electronic density of states can occur with monolayers of metal coverage.⁵⁻⁸ These changes have been attributed to chemical reactions between the metal and semiconductor

atoms and the formation of an interfacial silicide layer. In this Letter, we report a quantitative determination of the interface width of the Ni-Si system and its development as a function of metal coverage. Our result also shows that the substrate temperature during or after the metal deposition can substantially alter the interfacial reactivity.

The megaelectronvolt ion-backscattering and transmission channeling techniques have been



$$\vec{V}_g \cdot \vec{B}_0 > 0$$



$$\vec{V}_g \cdot \vec{B}_0 < 0$$

FIG. 3. (a) Integrated Rogowski loop for current measurements. (b) Current generated by a 200-W, 120- μ s rf pulse with $\vec{V}_g \cdot \vec{B}_0 > 0$. (\vec{V}_g denotes the group velocity of the wave.) Top trace shows the rf pulse and bottom trace shows the Rogowski-loop signal. (c) Same, but with $\vec{V}_g \cdot \vec{B}_0 < 0$.